Fast 3D Volume Super Resolution Using an Analytical Solution for l2-l2 Problems

Rose Sfeir [1], Bilal Chebaro[1], Charbel Julien[1]
[1] Computer Science Department, Lebanese University, Hadath, Lebanon
Email: rosesfeir@gmail.com, bchebaro@ul.edu.lb, charbeljulien@hotmail.com

Abstract: In Endodontics, dentists need a good visualization of dental root canals as found in Cone Beam Computed Tomography (CBCT) dental volumes to diagnose and prevent the development of some anomalies. These CBCT dental volumes, however, suffer from low resolution. In order, to enhance their resolution, we need to apply a super-resolution technique. In this paper, we propose a new 3D super resolution algorithm based on a linear model, consisting of a blurring operator and a decimation operator, which is an extension of Zhao's work [1] in 3D, taking the low-resolution volume as an input and producing the high-resolution volume as an output. We present a generalization of the 2D Super-Resolution problem into a 3D Super-Resolution problem as we apply it to 3D dental volume. Our new Super-Resolution algorithm as applied to dental CBCT volumes is a direct method aiming to get the exact solution with a short computation time. Results show an improvement in the resolution of the CBCT in a short time in comparison with Zhao's work, which was applied to CBCT dental volumes slice by slice, [2].

Index Terms: Super Resolution, Inverse Problems, CBCT, MCT, Endodontics.

1. Introduction

Endodontics requires a full visualization of the root canal to successfully treat the dental pulp cavity. Dentists use Cone Beam Computed Tomography (CBCT), a medical imaging technique consisting of X-ray computed tomography with conical divergent X-rays rotating around the head of the patient to reconstruct the 3D structure of the teeth. CBCT has become increasingly important in implant dentistry for treatment planning and diagnosis. Dentists need a better visualization of the canal to diagnose and prevent the development of some anomalies. For this purpose, increasing the image resolution should significantly improve the diagnostic ability for a more accurate corrective treatment. The reliable technique for imaging the root canal anatomy is Micro computed tomography (μCT).

While the benefits of this technique are a high spatial resolution and high contrast 3D images, its disadvantages are a limited field of view, with high irradiation doses, a limited access and long acquisition time. Cone Beam Computed Tomography (CBCT) is an interesting alternative to μCT, as it is able to image the dento-maxillo-facial structures using a conic X-ray beam moving around the patient's head. CBCT has a larger field of view, a reduced acquisition time and lower irradiation doses, making it suitable for clinical applications. Despite its numerous advantages, CBCT suffers from its insufficient spatial resolution, which prevents it, for the moment, from exploring the root canal system quantitatively. The objective of this paper is to evaluate the potential of our new Super-Resolution (SR) method, which aims to enhance the resolution of CBCT volumes. It takes the low-resolution volume as an input and produces the high-resolution volume as an output. A reconstruction-based Super-Resolution (SR) method using total variation regularization is evaluated on extracted teeth. The results show the interest of SR in improving the root canal detection on CBCT data.

The remainder of the paper is organized as follows. In Section 2, we present the literature review. In Section 3, we present the volume super resolution problem in 3D, the computation of the solution and our algorithm in Section 4. Our various experiments and results show the efficiency of the proposed 3D Super-resolution method in Section 5. Conclusion is described in Section 6. Finally, we present the proofs of the property of the decimation matrix and the property of the blurring matrix.

2. Related Work

We introduce the Super-Resolution technique that aims at reconstructing a higher resolution image from observed low-resolution images, which are divided into two categories: multi-image super-resolution and single image super-resolution. Multi-image Super-resolution is a technique consisting of generating a high-resolution image from multiple low-resolution images, whereas the Single Image Super-Resolution is a method that generates a high-resolution image from its low-resolution image. SR has very different applications: satellite image processing, medical imaging,

microscopy image processing, multimedia industry and video enhancement, astrological studies. We focus in this paper on single image super-resolution techniques. In the literature, we find three types of single image super-resolution techniques: interpolation-based, learning-based and reconstruction based, [3,4]. First, interpolation-based techniques are the simplest way to get a high-resolution image based on linear filtering, as it is seen in the nearest neighbor interpolation, the bilinear interpolation and the bicubic interpolation, [5,6,7]. Second, in learning-based methods, the lost details in a low-resolution image can be retrieved from a dictionary formed by the high-resolution image [3,8,9]. The effectiveness of this method is based on the good choice of the training dataset. Recently, deep learning algorithms have been used to solve super-resolution problems despite their high computational complexity, [10,11]. These algorithms can erase, change or even add some details to the image since they are conceived as a system to make decision. It is not trivial to get the good reconstruction. Third, reconstruction based algorithms enforce the constraint of having a consistency between the version of the high-resolution image and its low-resolution image according to predefined values [12,13]. The problem turns out to be an optimization problem with a specific optimization, and the solution is guaranteed. We cite some reconstruction-based methods: the first order gradient-based methods [3,4,14], the iterative shrinkage thresholding based algorithms [15], and the proximal gradient methods. Many algorithms rely on the Alternating Direction Methods of Multipliers (ADMM) framework, an algorithm that solves convex optimization problems by breaking them into smaller pieces, each of which then become easier to handle, such as in [12,16,17,18]. The ADMM framework is used when we need to minimize a convex function subject to a condition (usually the regularization). In [2], we showed the potential of super-resolution (SR) to enhance the resolution of CBCT images with an improvement of the root canal segmentation. We have reconstructed our high-resolution volume by applying a super-resolution technique (based on reconstruction-based approaches) for every slice. We have developed a 3D super resolution technique based on reconstruction-based approaches for enhancing the resolution in CBCT, instead of working slice by slice. In the literature, Feng Shi developed a method for 3D super-resolution that considers the low-resolution volume as a blurred, noisy and down sampled version of the high-resolution volume to be estimated. He modeled the low-resolution volume as a 3D tensor. His method takes into consideration two regularizations: the first one is total variation, and the second one is low rank regularization. They solve the total variation problem by applying a gradient descent method [19].

3. Background

A. *Super-Resolution problem*

We present the Super-Resolution problem in a 3D case: We express y as the low-resolution volume,

$$y = SHx + n \tag{1}$$

viewed as a high-resolution volume x, blurred and downsampled with an additive white gaussian noise.

$$y \in \square^{N_l \times 1}, \ N_l = m_l \times n_l \times o_l \tag{2}$$

$$x \in \square^{N_h \times 1}, \ N_h = m_h \times n_h \times o_h. \tag{3}$$

such that x is the high-resolution volume to be estimated, $n \in \square^{N_l \times 1}$, n is an independent identically distributed (i.i.d.) (AWGN), S is the decimation matrix, $S \in \square^{N_l \times N_h}$ and H is the blurring matrix, block circulant $H \in \square^{N_h \times N_h}$. This property is used in the following references [3,9,20,21]. We can express the H block circulant, which is diagonalizable into Fourier, as:

$$H = F^{Inv} \Lambda F \tag{4}$$

such that

$$\Lambda = diag\{Fh\} \in \square^{N_h \times N_h} \tag{5}$$

a diagonal matrix whose diagonal elements are the Fourier coefficients of the first column of the blurring matrix H denoted as h and

$$H^* = F^{Inv} \Lambda^* F \tag{6}$$

Some relations:

$$N_h = N_l \times d^3 \tag{7}$$

$$m_h = m_l \times d$$
$$n_h = n_l \times d \tag{8}$$
$$o_h = o_l \times d$$

Our goal is to reconstruct the high-resolution volume x from the low-resolution volume y. For this reason, we need to solve the super resolution problem:

$$\min_x \frac{1}{2} \underbrace{\left\| y - SHx \right\|_2^2}_{\text{data fidelity}} + \tau \underbrace{\phi(Ax)}_{\text{regularization}} \tag{9}$$

We choose to use the total variation regularization:

$$\phi(Ax) = \left\| x \right\|_{TV} \tag{10}$$
$$\text{such that } Ax = u$$

The problem is rewritten as:

$$\min_x \frac{1}{2} \left\| y - SHx \right\|_2^2 + \tau\phi(Ax) \tag{11}$$
$$\text{subject to } Ax = u$$

With total variation regularization, A can be expressed as:

$$A = \left[D_h^T, D_v^T, D_z^T \right] \in \square^{3N_h \times N_h} \tag{12}$$

Where D_h, D_v, D_z are three BCCB matrices corresponding to the horizontal and vertical and through z direction discrete differences of a volume. So, D_h, D_v, D_z can be decomposed in the frequency domain

$$D_h = F^{Inv} \Sigma_h F$$
$$D_v = F^{Inv} \Sigma_v F \tag{13}$$
$$D_z = F^{Inv} \Sigma_z F$$

$A^* A$ could not be invertible; for this reason, we have added a small norm and Ψ becomes:

$$\Psi = \left(\Sigma_h^* \Sigma_h + \Sigma_v^* \Sigma_v + \Sigma_z^* \Sigma_z + \sigma I_{N_h} \right)^{-1} \tag{14}$$

In order to solve problem 11, we need to apply ADMM framework as explained in Algorithm 1.
The Augmented Lagrangian function associated with this problem is

$$L(x, u, \lambda) = \frac{1}{2} \left\| y - SHx \right\|_2^2 + \tau\phi(u) + \lambda^T \left(Ax - u \right)$$
$$+ \frac{\mu}{2} \left\| Ax - u \right\|_2^2 \tag{15}$$

Or equivalently

$$L(x,u,d) = \frac{1}{2}\|y - SHx\|_2^2 + \tau\phi(u)$$
$$+ \frac{\mu}{2}\|Ax - u + d\|_2^2 \tag{16}$$

We also need to minimize $L(x,u,d)$ with respect to x and u and update the scaled dual variable d iteratively as summarized in Algorithm 1. The third step that is updating the HR volume x can be solved analytically using Theorem 1. The variable u is updated at the fourth step using the Moreau proximity operator whose definition is given by:

$$prox_{\lambda,\phi}(v) = \frac{\arg\min\phi(x)}{x} + \frac{1}{2\lambda}\|x - v\|^2 \tag{17}$$

We start by the l2-l2 regularization in order to solve the first step of this algorithm. We need to solve the first step of the algorithm, particularly this equation

$$\min_{x} \frac{1}{2}\|y - SHx\|_2^2 + \tau\|Ax - v\|_2^2 \tag{18}$$

We call it the analytical solution.

B. Computation of the solution

We use two basic assumptions about the blurring and decimation operators [1]. These assumptions have been widely used for image deconvolution or image SR problems and are necessary for the proposed fast SR framework in order to accelerate the computation time of the algorithm. We denote:

$$\underline{S} = S^*S \tag{19}$$

Through derivation, we solve this problem, see Equation (18). We get:

$$-\left(SH\right)^*\left(y - SHx\right) + 2\tau A^*\left(Ax - v\right) = 0$$
$$x\left(H^*S^*SH + 2\tau A^*A\right) = H^*S^*y + 2\tau A^*v \tag{20}$$
$$\hat{x} = \left(H^*\underline{S}H + 2\tau A^*A\right)^{-1}\left(H^*S^*y + 2\tau A^*v\right)$$

We show that the decimation matrix S has the following property in the Fourier Domain:

$$F\underline{S}F^{Inv} = \frac{1}{d^3}\left(J_d \otimes I_{o_l}\right) \otimes \left(J_d \otimes I_{n_l}\right)$$
$$\otimes \left(J_d \otimes I_{m_l}\right) \tag{21}$$

see subsection A). Then, we get:

$$\hat{x} = F^{Inv}\left(\frac{1}{d^3}\underline{\Lambda}^*\underline{\Lambda} + 2\tau FA^*AF^{Inv}\right)^{-1}$$
$$F\left(H^*S^*y + 2\tau A^*v\right) \tag{22}$$

while replacing $F \underline{S} F^{Inv}$ by its property and H
by its expression on Fourier Domain (see Equations 4, 6). In fact, from (20)

$$\hat{x} = \left(F^{Inv} \Lambda^* \times \frac{1}{d^3} J \Lambda F + 2\tau A^* A \right)^{-1}$$
$$\left(H^* S^* y + 2\tau A^* v \right)$$

(23)

With

$$J = \left(J_d \otimes I_{o_l} \right) \otimes \left(J_d \otimes I_{n_l} \right) \otimes \left(J_d \otimes I_{m_l} \right)$$

(24)

And

$$\Lambda^* F \underline{S} F^{Inv} \Lambda = Cc$$

(25)

Let

$$K = \left(\left(1_d 1_d^T \right) \otimes \left(I_{o_l} I_{o_l} \right) \right) \otimes \left(\left(1_d 1_d^T \right) \otimes \left(I_{n_l} I_{n_l} \right) \right)$$
$$\otimes \left(\left(1_d 1_d^T \right) \otimes \left(I_{m_l} I_{m_l} \right) \right)$$

(26)

$$Cc = \frac{1}{d^3} \Lambda^* \left(J_d \otimes I_{o_l} \right) \otimes \left(J_d \otimes I_{n_l} \right) \otimes \left(J_d \otimes I_{m_l} \right) \Lambda$$

$$= \frac{1}{d^3} \Lambda^* K \Lambda$$

$$= \frac{1}{d^3} \Lambda^* \left(\left(1_d \otimes I_{o_l} \right) \left(1_d^T \otimes I_{o_l} \right) \right) \otimes \left(\left(1_d \otimes I_{n_l} \right) \left(1_d^T \otimes I_{n_l} \right) \right)$$
$$\otimes \left(\left(1_d \otimes I_{m_l} \right) \left(1_d^T \otimes I_{m_l} \right) \right) \Lambda$$

$$= \frac{1}{d^3} \left(\Lambda^* \left[I_{o_l}, \cdots, I_{o_l} \right]^T \left[I_{o_l}, \cdots, I_{o_l} \right] \right)$$
$$\otimes \left(\left[I_{n_l}, \cdots, I_{n_l} \right]^T \left[I_{n_l}, \cdots, I_{n_l} \right] \right)$$
$$\otimes \left(\left[I_{m_l}, \cdots, I_{m_l} \right]^T \left[I_{m_l}, \cdots, I_{m_l} \right] \Lambda \right)$$

$$= \frac{1}{d^3} \left(\Lambda^* \underbrace{\left[I_{o_l}, \cdots, I_{o_l} \right]^T \left[I_{n_l}, \cdots, I_{n_l} \right]^T \otimes \left[I_{m_l}, \cdots, I_{m_l} \right]^T}_{d^3} \right)$$

$$\left(\underbrace{\left[I_{o_l}, \cdots, I_{o_l} \right] \otimes \left[I_{n_l}, \cdots, I_{n_l} \right] \otimes \left[I_{m_l}, \cdots, I_{m_l} \right]}_{d^3} \Lambda \right)$$

(27)

We get:

$$A = \frac{1}{d^3} \underline{\Lambda}^* \underline{\Lambda}$$

(28)

Note that $\underline{\Lambda} \in \square^{m_l n_l o_l \times mno}$,

$$\underline{\Lambda} = \left[I_{o_l}, \cdots, I_{o_l} \right] \otimes \left[I_{n_l}, \cdots, I_{n_l} \right] \otimes \left[I_{m_l}, \cdots, I_{m_l} \right] \Lambda$$

$$= \left[I_{o_l n_l m_l}, \cdots, I_{o_l n_l m_l} \right] \Lambda$$

$$= \left[I_{o_l n_l m_l}, \cdots, I_{o_l n_l m_l} \right] \begin{bmatrix} \Lambda_1 & \cdots & \cdots & \cdots \\ \vdots & \Lambda_2 & \cdots & \cdots \\ \vdots & \vdots & \ddots & \cdots \\ \vdots & \vdots & \vdots & \Lambda_{d^3} \end{bmatrix}$$

$$\underline{\Lambda} = \left[\Lambda_1, \cdots, \Lambda_{d^3} \right] \tag{29}$$

$$\text{So, } \hat{x} = F^{Inv} \left(\frac{1}{d^3} \underline{\Lambda}^* \underline{\Lambda} + 2\tau F A^* A F^{Inv} \right)^{-1} F r \tag{30}$$

with

$$r = H^* S^* y + 2\tau A^* v \tag{31}$$

This solution is hard to be implemented in MATLAB, which requires one more simplified. For this reason, we have applied Woodbury's formula, [1].

Theorem 1: When Assumptions 1 and 2 are satisfied, [1] the solution of the problem can be computed using the following closed-form expression

$$\hat{x} = \frac{1}{2\tau} F^{Inv} \psi F r - \frac{1}{2\tau} F^{Inv} \psi \underline{\Lambda}^* \left(2\tau d^3 I_{N_l} + \underline{\Lambda} \psi \underline{\Lambda}^* \right)^{-1} \tag{32}$$
$$\underline{\Lambda} \psi F r$$

with equation (31)

$$\psi = F \left(A^* A \right)^{-1} F^{Inv} \tag{33}$$

Proof 1: While applying Woodbury's formula with: Equation (33),

$$A_1 = 2\tau F A^* A F^{Inv}$$
$$A_2 = \underline{\Lambda}^*$$
$$A_3 = \frac{1}{d^3} I_{N_l} \tag{34}$$
$$A_4 = \underline{\Lambda}$$

We note

$$Q = \left(\frac{1}{d^3} \underline{\Lambda}^* \underline{\Lambda} + 2\tau F A^* A F^{Inv} \right)^{-1} \tag{35}$$

We get:

$$Q = \frac{1}{2\tau} F \left(A^* A \right)^{-1} F^{Inv} - \frac{1}{2\tau} \psi \underline{\Delta}^* \left(d^3 I_{N_l} + \underline{\Delta} \left(\frac{1}{2\tau} \psi \right) \underline{\Delta}^* \right)^{-1}$$

$$\underline{\Delta} \times \left(\frac{\psi}{2\tau} \right)$$

$$= \frac{\psi}{2\tau} - \frac{\psi}{2\tau} \underline{\Delta}^* \left(\frac{2\tau d^3 I_{N_l} + \underline{\Delta} \psi \underline{\Delta}^*}{2\tau} \right)^{-1} \underline{\Delta} \times \frac{\psi}{2\tau}$$

$$= \frac{\psi}{2\tau} - \frac{\psi}{2\tau} \underline{\Delta}^* \times 2\tau \times \left(2\tau d^3 I_{N_l} + \underline{\Delta} \psi \underline{\Delta}^* \right)^{-1} \underline{\Delta} \times \frac{\psi}{2\tau}$$

$$= \frac{\psi}{2\tau} - \frac{\psi}{2\tau} \underline{\Delta}^* \times \left(2\tau d^3 I_{N_l} + \underline{\Delta} \psi \underline{\Delta}^* \right)^{-1} \underline{\Delta} \psi$$

(36)

So,

$$\hat{x} = F^{Inv} \left(\frac{1}{d^3} \underline{\Delta}^* \underline{\Delta} + 2\tau F A^* A F^{Inv} \right)^{-1} F r$$

$$= F^{Inv} \left(\frac{\psi}{2\tau} - \frac{\psi}{2\tau} \underline{\Delta}^* \times \left(2\tau d^3 I_{N_l} + \underline{\Delta} \psi \underline{\Delta}^* \right)^{-1} \underline{\Delta} \psi \right) F r$$

$$= \frac{1}{2\tau} F^{Inv} \psi F r - \frac{1}{2\tau} F^{Inv} \psi \underline{\Delta}^* \left(2\tau d^3 I_{N_l} + \underline{\Delta} \psi \underline{\Delta}^* \right)^{-1}$$

$$\underline{\Delta} \psi F r$$

(37)

We obtain a simplified solution that is easy to implement in MATLAB In case

$$A = I_{N_h}$$

(38)

Then

$$\psi = I_{N_h}$$

(39)

And

$$\hat{x} = \frac{1}{2\tau} r - \frac{1}{2\tau} F^{Inv} \underline{\Delta}^* \left(2\tau d^3 I_{N_l} + \underline{\Delta} \underline{\Delta}^* \right)^{-1} \underline{\Delta} F r$$

(40)

This is the computation of the analytical solution, and we have written the algorithm of its computation in Algorithm 2. We choose to use the total variation regularization, based on ADMM framework, and we present this scheme in Algorithm 1. And we introduce our new 3D Super resolution algorithm based on the ADMM method in Algorithm 3.

Algorithm 1: Fast Super-Resolution (FSR) Scheme

Input : $y, H, S, \overline{x}, \tau, d$

1 Set $l = 0$, choose $\mu > 0$, u^0, d^0;

2 **Repeat**

3 $x^{l+1} = \underset{x}{\arg\min} \left\| y - SHx \right\|_2^2 + \mu \left\| Ax - u^l + d^l \right\|_2^2$

4 $u^{l+1} = \underset{u}{\arg\min} \tau \phi(u) + \frac{\mu}{2} \left\| Ax^{l+1} - u + d^l \right\|_2^2$

5 $d^{l+1} = d^l + \left(Ax^{l+1} - u^{l+1} \right)$

6 **until** stopping criterion is satisfied.

Algorithm 2: Fast Super-Resolution (FSR) with Volume Domain l2-Regularization : Implementation of the Analytical Solution (see Equation 11)

Input : $y, H, S, \overline{x}, \tau, d$

1 $H = F^{Inv} \Lambda F$ // Factorization of H (FFT of the blurring kernel)

2 $\underline{\Lambda} = \left[\Lambda_1, \Lambda_2, \cdots, \Lambda_{d^3} \right]$ // Compute $\underline{\Lambda}$

3 $Fr = F \left(H^* S^* y + 2\tau \overline{x} \right)$; // Calculate FFT of r denoted as Fr

4 $x_f = \left(\Lambda_H \left(2\tau d^3 I_{N_l} + \underline{\Lambda}\,\underline{\Lambda}^* \right)^{-1} \underline{\Lambda} \right) Fr$; // Hadamard or (entrywise) product in frequency domain.

5 $\widehat{x} = \dfrac{1}{2\tau} \left(r - F^{Inv} x_f \right)$; // Compute the analytical solution

Output: $\widehat{x}$

---

4.   Proposed Algorithm

Algorithm 3 represents the proposed algorithm. Firstly, we take the low resolution volume as an input with a 3D known point spread function, we solve an inverse problem through ADMM framework, and then we find the high resolution volume, generated as an output.

Algorithm 3: 3D FSR with TV Regularization (our new algorithm)

Input : $y, H, S, \tau, d, D_h, D_v, D_z$

1 Set $l = 0$, choose $\mu > 0, d^0, u^0$; // Factorization of matrix H

2 $H = F^{Inv} \Lambda F$;

3 $\underline{\Lambda} = \left[\Lambda_1, \Lambda_2, \cdots, \Lambda_{d^3} \right]$ // Factorization of matrices D_h, D_v, and D_z

4 $D_h = F^{Inv} \Sigma_h F$

5 $D_v = F^{Inv} \Sigma_v F$

6 $D_z = F^{Inv} \Sigma_z F$

7 $\psi = \left(\Sigma_h^* \Sigma_h + \Sigma_v^* \Sigma_v + \Sigma_h^* \Sigma_h \right)^{-1}$

8 **Repeat**

9 // Update x using Theorem 1

10 $\rho_h = u_h^l - d_h^l$;

11 $\rho_v = u_v^l - d_v^l$;

12 $\rho_z = u_z^l - d_z^l$;

13 $Fr = F \left(H^* S^* y + \mu D_h \rho_h + \mu D_v \rho_v + \mu D_z \rho_z \right)$;

$$14 \quad x_f = \left(\psi \underline{\Lambda}^* \left(\mu d^3 I_{N_l} + \underline{\Lambda} \psi \underline{\Lambda}^* \right)^{-1} \underline{\Lambda} \psi \right) Fr;$$

$$15 \quad x^{l+1} = \frac{1}{\mu} F^{Inv} \psi \, Fr - \frac{1}{\mu} F^{Inv} x_f;$$

16 // Update u using the vector-soft thresholding operator

$$17 \quad v = \left[D_h x^{l+1} + d_h^l, D_v x^{l+1} + d_v^l, D_z x^{l+1} + d_z^l \right];$$

$$18 \quad u^{l+1}[i] = \max \left\{ 0, \left\| v[i] - \frac{\tau}{\mu} \right\|_2 \right\} \frac{v[i]}{\|v[i]\|^2}$$

19 // Update the dual variables d

$$20 \quad d^{l+1} = d^l + \left(Ax^{l+1} - u^{l+1} \right)$$

21 $\quad l = l + 1$

22 until stopping criterion is satisfied;

Output: $\hat{x} = x^l$
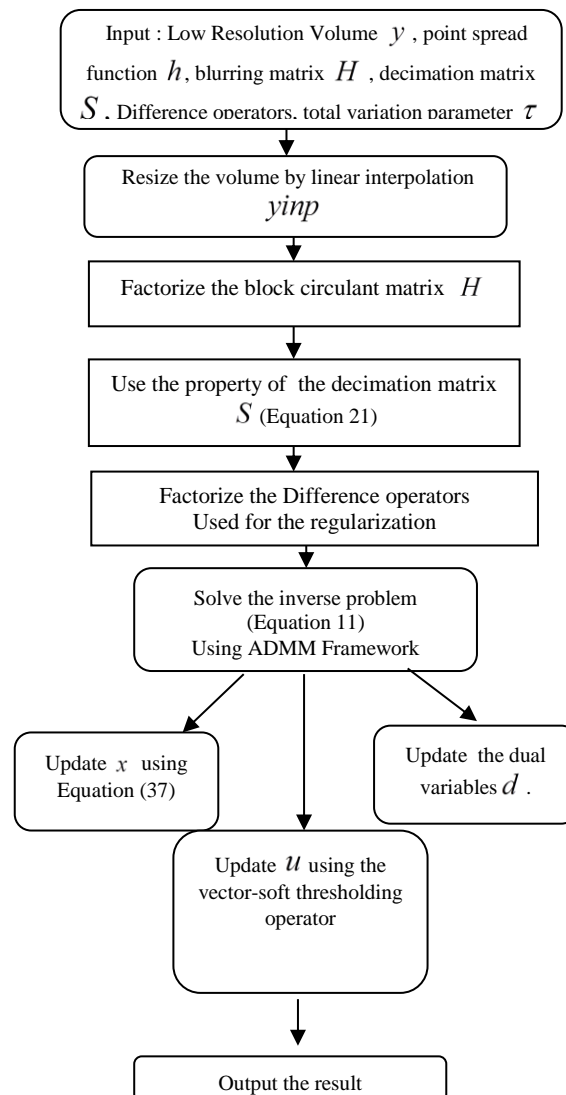
Fig. The architecture of the algorithm

5.   Experiment simulation and result analysis

This section shows the efficiency of the proposed Fast 3D Super- Resolution method. All the experiments were performed using MATLAB 2018a on a computer with Windows 10, Intel(R) Core(TM) i7-5500U CPU @2.40GHz and 12GB RAM. The performances of the SR algorithms are evaluated both visually and quantitatively in terms of the following metric: peak signal-to noise ratio (PSNR). The definition of this metric, widely used to evaluate image reconstruction methods, is given below:

- Peak Signal to Noise Ratio:

$$PSNR = 20\log_{10} \frac{\max(x, \hat{x})}{\sqrt{\|x - \hat{x}\|^2}} \tag{41}$$

where x and $\hat{x}$ are the ground truth (reference / HR volume) and the restored SR volume, respectively. First, we present the result on a μCT Incisor tooth with a total variation regularization. We tried different values of the TV regularization parameters (τ, μ) and found the optimal ones. The computing time is less than 50 seconds (fig.1.). Then, we present the CBCT volume, considered as low-resolution, which is blurred and decimated, and we obtain the CBCT SR volume with a total variation regularization (fig.2.). We tried to define the convenient point spread function with the optimal total variation regularization parameters. In fig.4. we show the horizontal, sagittal and coronal slices for CBCT SR that only 3D Super-Resolution techniques can provide. Finally, in figures 5 and 6, we show that our 3D Super-Resolution method gives higher PSNR compared to the 2D method with an approximately similar timing, and after a few number of iterations our algorithm converges.

Table1. Parameters Used While Applying Our Method on A MCT Incisor with a TV Regularization.

Parameter	Value
Tau	0.01
Mu	0. 5
Size of the low-resolution volume	150*150*150
Size of the point spread function	5*5*5
Size of the noise	150*150*150
Tolerance	1e-3

Table2. Parameters Used While Applying Our Method on A CBCT Incisor with a TV Regularization.

Parameter	Value
Tau	0.03
Mu	0.15
Size of the low-resolution volume	75*75*75
Size of the point spread function	7*7*7
Size of the noise	75*75*75
Tolerance	1e-3
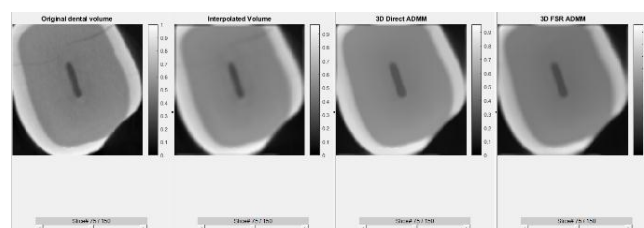
Fig.1. Result of Incisor tooth with a total variation regularization.
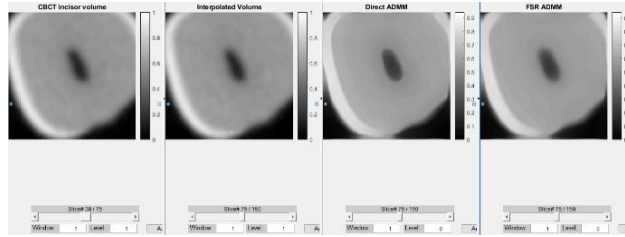
Fig.2. Result of CBCT Incisor tooth with a total variation regularization.
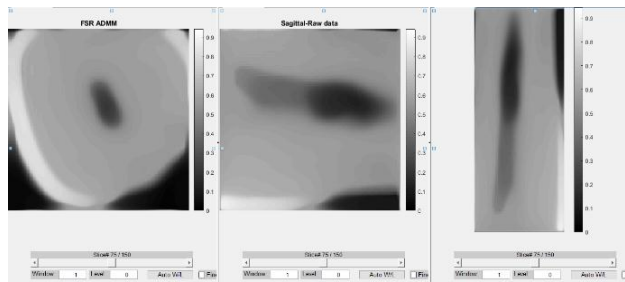
Fig.3. Result of CBCT Incisor tooth with a total variation regularization.
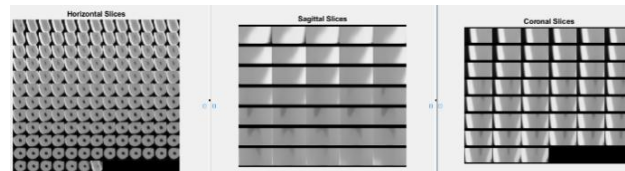
Fig.4. Result of CBCT Incisor tooth with a total variation regularization: Horizontal, Sagittal and Coronal Slices.
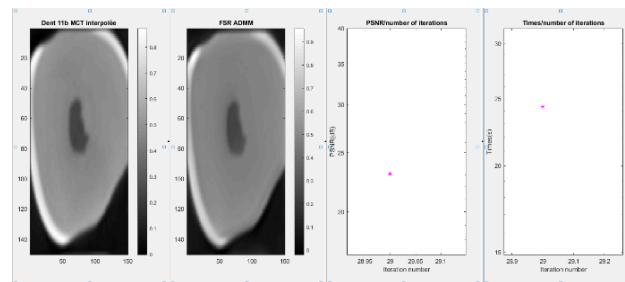
Fig.5. Result of MCT Incisor tooth with a total variation regularization, 2D method.
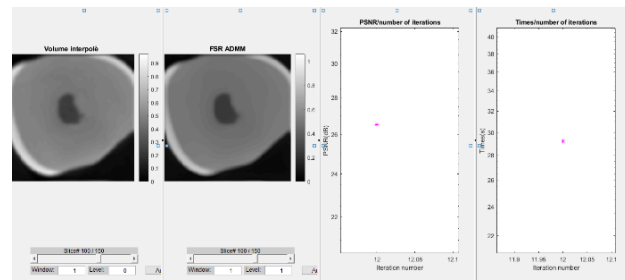
Fig.6. Result of MCT Incisor tooth with a total variation regularization, 3D method.
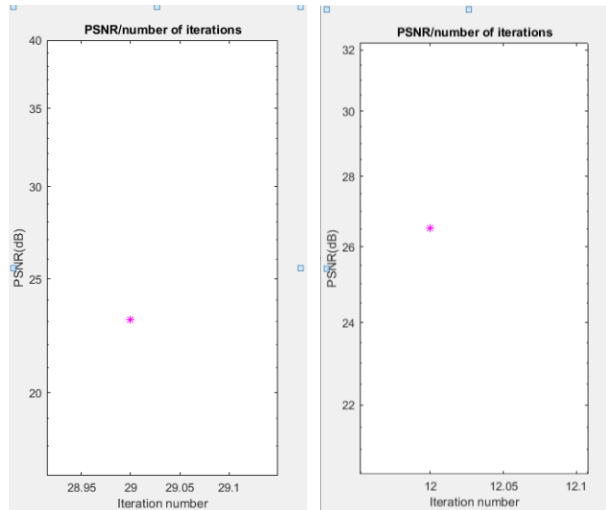
Fig.7. Result of the PSNR of MCT Incisor tooth with a total variation regularization, 2D method (left), 3D method (right).
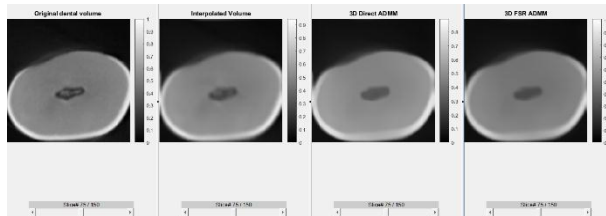
Fig.8. Result of MCT Incisor tooth with a total variation regularization, 3D method
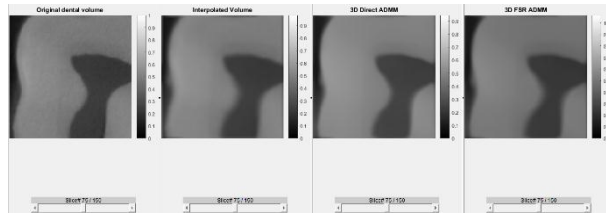
Fig.9. Result of MCT Molar tooth with a total variation regularization, 3D method
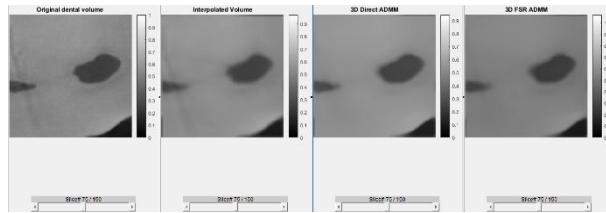
Fig.10. Result of MCT Molar tooth with a total variation regularization, 3D method
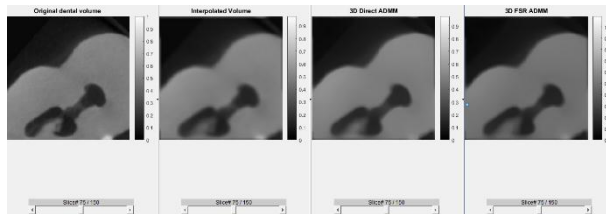
Fig.11. Result of MCT Molar tooth with a total variation regularization, 3D method

In figure [1], we present The MCT Incisor Volume, we blur it and down sample it and we reconstruct it through our Direct ADMM 3D Method and FSR ADMM 3D Method. The results are similar to the MCT Incisor Volume. All the parameters are summarized in Table [1]. In figure [2], we used CBCT Incisor volume, considered as low-resolution volume, we got the high resolution volume by using our 3D SR method, Direct ADMM in 3D and FSR ADMM in 3D. We can see the enhancement of the resolution. All the parameters are described in Table [2]. In figure [3], we can see in this result the reconstructed high resolution volume seen by different directional slices. In figure [4], we show all slices

of the reconstructed high-resolution volume: horizontal, sagittal and coronal slices. In figure [5], we show in this result the PSNR and the computing time of the FSR algorithm slice by slice taking MCT images (slice by slice) as input. In figure [6], we show the PSNR and the computing time of our FSR algorithm taking MCT volume as input. We can see in figure [7] that with our method the PSNR is greater than the method slice by slice with approximately same timing. In figures 8, 9, 10, 11 we show the effect of our super resolution technique on different types of dental volumes.

6. Conclusion

This work presents a 3D super-resolution method based on a linear model that is formed by a blurring operator and a decimation operator, both having some properties in Fourier leading to an acceleration of the computational time of the algorithm. We have successfully applied this method to a dental medical volume, in order to enhance the resolution of CBCT dental volumes, which helps to detect the root canal anatomy, containing the full information of the health of the tooth. In this method, we use total variation regularization to smoothe the solution. In future research, we could apply another type of regularization such as wavelets. We could also modify the modelization of the problem or work with blind approaches in order to estimate the point spread function in our further research.

Appendix

Property Of The Decimation Matrix

In this subsection, we present the proofs of the properties of the decimation matrix in 1D, 2D and 3D cases. Reminder: The mask S^*S is a mask of size $N_h \times N_h$ having ones at the sampled positions and zeros elsewhere. In Superfast joint demosaicing and super-resolution, Glazitov et al [22] present an explicit form of the decimation matrix S.

Proof 2: An operator that downsamples a vector of size n by a factor d is written as:

$$D_d = I_{n/d} \otimes e_{1,d}^T \tag{42}$$

where $e_{1,d}^T$ is the first line of the identity matrix I_d.

In 1D,

$$S = \left(I_{n/d} \otimes e_{1,d}^T \right) \tag{43}$$

$$S^* = \left(I_{n/d} \right)^* \otimes \left(e_{1,d}^T \right)^* \tag{44}$$

$$
\begin{aligned}
S^*S &= \left[\left(I_{n/d} \right)^* \otimes \left(e_{1,d}^T \right)^* \right]\left[\left(I_{n/d} \otimes e_{1,d}^T \right) \right] \\
&= \left[I_{n/d}^* \times I_{n/d} \right] \otimes \left[e_{1,d} \times e_{1,d}^T \right] \\
&= I_{n/d} \otimes \begin{bmatrix} 1 & 0 & \cdots & 0 \\ 0 & 0 & \cdots & 0 \\ \vdots & \vdots & \ddots & \vdots \\ 0 & 0 & \cdots & 0 \end{bmatrix}
\end{aligned}
\tag{45}
$$

The proof in 1D is explained in [23].
We get,

$$FS^*SF^{Inv} = F^{Inv}S^*SF = \frac{1}{d}\left(J_d \otimes I_{n_l} \right) \tag{46}$$

Proof 3: The 2D downsampling by a d factor becomes

$$D_{d.d} = D_d \otimes D_d = I_{n/d} \otimes e_{1,d}^T \otimes I_{n/d} \otimes e_{1,d}^T \tag{47}$$

$$S = \left(I_{n/d} \otimes e_{1,d}^T \right) \otimes \left(I_{n/d} \otimes e_{1,d}^T \right) \tag{48}$$

$$
\begin{aligned}
S^* &= \left[\left(I_{n/d} \otimes e_{1,d}^T \right) \otimes \left(I_{n/d} \otimes e_{1,d}^T \right) \right]^* \\
&= \left[\left(I_{n/d} \otimes e_{1,d}^T \right) \right]^* \otimes \left[\left(I_{n/d} \otimes e_{1,d}^T \right) \right]^* \\
&= \left[\left(I_{n/d} \otimes e_{1,d}^T \right) \right] \otimes \left[\left(I_{n/d} \otimes e_{1,d}^T \right) \right]
\end{aligned}
\tag{49}
$$

$$
\begin{aligned}
S^*S &= \left[\left(I_{n/d} \otimes e_{1,d} \right) \otimes \left(I_{n/d} \otimes e_{1,d} \right) \right]\left[\left(I_{n/d} \otimes e_{1,d}^T \right) \otimes \left(I_{n/d} \otimes e_{1,d}^T \right) \right] \\
&= \left[\left(I_{n/d} \otimes e_{1,d} \right) \times \left(I_{n/d} \otimes e_{1,d}^T \right) \right]\left[\left(I_{n/d} \otimes e_{1,d} \right) \times \left(I_{n/d} \otimes e_{1,d}^T \right) \right] \\
&= \left[\left(I_{n/d} \times I_{n/d} \right) \otimes \left(e_{1,d} \times e_{1,d}^T \right) \right] \otimes \left[\left(I_{n/d} \times I_{n/d} \right) \otimes \left(e_{1,d} \times e_{1,d}^T \right) \right] \\
&= \left[E_1 + E_{1+d} + \cdots + E_{1+\left(n/d-1\right)d} \right] \otimes \left[E_1 + E_{1+d} + \cdots + E_{1+\left(n/d-1\right)d} \right]
\end{aligned}
\tag{50}
$$

$$
\begin{aligned}
F^{Inv}\left(E_i \otimes E_i \right) F &= \left(E_i F \right)^{Inv} \otimes \left(E_i F \right) \\
&= \left(\left(E_i F \right)^{Inv} E_i F \right) \otimes \left(F^{Inv} E_i F \right) \\
&= \left(F^{Inv} E_i F \right) \otimes \left(F^{Inv} E_i F \right) \\
&= \left(\frac{1}{d}\left(J_d \otimes I_{n_l} \right) \right) \otimes \left(\frac{1}{d}\left(J_d \otimes I_{n_l} \right) \right)
\end{aligned}
\tag{51}
$$

So,

$$FS^*SF^{Inv} = F^{Inv}S^*SF = \frac{1}{d^2}\left(J_d \otimes I_{n_l} \right) \otimes \left(J_d \otimes I_{n_l} \right) \tag{52}$$

And our contribution is that we extend this property to 3D. The 3D downsampling by a d factor becomes

$$
\begin{aligned}
D_{d,d,d} &= D_d \otimes D_d \otimes D_d \\
&= I_{n/d} \otimes e_{1,d}^T \otimes I_{n/d} \otimes e_{1,d}^T \\
&\otimes I_{n/d} \otimes e_{1,d}^T
\end{aligned}
\tag{53}
$$

We justify the property of the decimation matrix in 3D:

$$F\underline{S}F^{Inv} = \frac{1}{d^3}\left(J_d \otimes I_{o_l} \right) \otimes \left(J_d \otimes I_{n_l} \right) \otimes \left(J_d \otimes I_{m_l} \right) \tag{54}$$

Proof 4: We consider the size of our volume: $m \times n \times o$ and $m = m_l \times d$, $n = n_l \times d$, and, $o = o_l \times d$.

$$S = D_{d,d,d} = D_d \otimes D_d \otimes D_d$$

$$= I_{m/d} \otimes e_{1,d}^T \otimes I_{n/d} \otimes e_{1,d}^T \otimes I_{o/d} \otimes e_{1,d}^T$$

$$= I_{m_l} \otimes e_{1,d}^T \otimes I_{n_l} \otimes e_{1,d}^T \otimes I_{o_l} \otimes e_{1,d}^T$$

$$= \left(I_{m/d} \otimes e_{1,d}^T \right) \otimes \left(I_{n/d} \otimes e_{1,d}^T \right) \otimes \left(I_{o/d} \otimes e_{1,d}^T \right)$$

(55)

$$S^* = \left[\left(I_{m/d} \otimes e_{1,d}^T \right) \otimes \left(I_{n/d} \otimes e_{1,d}^T \right) \otimes \left(I_{o/d} \otimes e_{1,d}^T \right) \right]^*$$

$$= \left[\left(I_{m/d} \otimes e_{1,d}^T \right) \right]^* \otimes \left[\left(I_{n/d} \otimes e_{1,d}^T \right) \right]^* \otimes \left[\left(I_{o/d} \otimes e_{1,d}^T \right) \right]^*$$

$$= \left[\left(I_{m/d} \otimes e_{1,d} \right) \right] \otimes \left[\left(I_{n/d} \otimes e_{1,d} \right) \right] \otimes \left[\left(I_{o/d} \otimes e_{1,d} \right) \right]$$

(56)

$$S^* S = \left[\left(I_{m/d} \otimes e_{1,d} \right) \otimes \left(I_{n/d} \otimes e_{1,d} \right) \otimes \left(I_{o/d} \otimes e_{1,d} \right) \right]$$

$$\left[\left(I_{m/d} \otimes e_{1,d}^T \right) \otimes \left(I_{n/d} \otimes e_{1,d}^T \right) \otimes \left(I_{o/d} \otimes e_{1,d}^T \right) \right]$$

$$= \left[\left(I_{m/d} \otimes e_{1,d} \right) \times \left(I_{m/d} \otimes e_{1,d}^T \right) \right] \otimes \left[\left(I_{n/d} \otimes e_{1,d} \right) \times \left(I_{n/d} \otimes e_{1,d}^T \right) \right]$$

$$\otimes \left[\left(I_{o/d} \otimes e_{1,d} \right) \times \left(I_{o/d} \otimes e_{1,d}^T \right) \right]$$

$$= \left[\left(I_{m/d} \times I_{m/d} \right) \otimes \left(e_{1,d} \times e_{1,d}^T \right) \right] \otimes \left[\left(I_{n/d} \times I_{n/d} \right) \otimes \left(e_{1,d} \times e_{1,d}^T \right) \right]$$

$$\otimes \left[\left(I_{o/d} \times I_{o/d} \right) \otimes \left(e_{1,d} \times e_{1,d}^T \right) \right]$$

$$= \left[E_1 + E_{1+d} + \cdots + E_{1+\left(m/d - 1 \right) d} \right] \otimes \left[E_1 + E_{1+d} + \cdots + E_{1+\left(n/d - 1 \right) d} \right]$$

$$\otimes \left[E_1 + E_{1+d} + \cdots + E_{1+\left(o/d - 1 \right) d} \right]$$

(57)

$$F^{Inv} \left(E_i \otimes E_i \otimes E_i \right) F = \left(E_i F \right)^{Inv} \otimes \left(\left(E_i \otimes E_i \right) \times F \right)$$

$$= \left(\left(E_i F \right)^{Inv} F \right) \otimes \left(F^{Inv} E_i \otimes E_i F \right)$$

$$= \left(F^{Inv} E_i F \right)$$

$$\otimes \left(\frac{1}{d^2} \left(J_d \otimes I_{n_l} \right) \otimes \left(J_d \otimes I_{n_l} \right) \right)$$

$$= \left(\frac{1}{d^3} \right)$$

$$\otimes \left(\left(J_d \otimes I_{m_l} \right) \otimes \left(J_d \otimes I_{n_l} \right) \otimes \left(J_d \otimes I_{o_l} \right) \right)$$

(58)

So,

$$FS^* S F^{Inv} = F^{Inv} S^* S F$$

$$= \frac{1}{d^3} \left(\left(J_d \otimes I_{m_l} \right) \otimes \left(J_d \otimes I_{n_l} \right) \otimes \left(J_d \otimes I_{o_l} \right) \right)$$

(59)

Property Of The Blurring Matrix

H from the 3D convolution is circulating per block, diagonalizable in Fourier, Equation (4)

Proof 5: In his course about Discrete Fourier Transform, André Eberhard [24], states the following property: The product of two circulating matrices that are associated to a vector is the circulating matrix that is associated to the periodic convolution product of these vectors. In fact, the circulating matrix relative to a filter h is written: C_h, so

$$FC_hF^{Inv} = D_{F(h)},\qquad(60)$$

with D the diagonal and the following properties are verified:

$$C_h = F^{Inv}D_{F(h)}F\qquad(61)$$

$$F^{Inv}D_HF = C_{F^{Inv}(H)}\qquad(62)$$

In our case:

$$y = h_{3D} * x = \left(h_{1D} \times h_{2D}\right) * x\qquad(63)$$

$$y = H_{1D} \times H_{2D} \times x = M \times x\qquad(64)$$

We want to prove that M is circulating per block:

$$M = C_{h_{1D}}C_{h_{2D}}\qquad(65)$$

$$\begin{aligned}FMF^{Inv} &= FC_{h_{1D}}F^{Inv}FC_{h_{2D}}F^{Inv}\\ &= D_{H_{1D}}D_{H_{2D}} = D_{H_{1D} \times H_{2D}}\end{aligned}\qquad(66)$$

$$\begin{aligned}M &= F^{Inv}D_{H_{1D} \times H_{2D}}F\\ &= C_{F^{Inv}(H_{1D} \times H_{2D})}\\ &= C_{F^{Inv}(H_{1D})*F^{Inv}(H_{2D})}\\ &= C_{h_{1D}*h_{2D}}\end{aligned}\qquad(67)$$

because the Fourier transform of the periodic convolution product of two vectors is the product of the Fourier Transform of both of the vectors.

Acknowledgment

References

[1] Zhao, N., Wei, Q., Basarab, A., Dobigeon, N., Kouamé, D., Tourneret J.-Y., Fast, J.-Y., Member, Student, Member, Senior, 2016. *Fast Single Image Super-Resolution Using a New Analytical Solution for l2–l2 Problems*. IEEE Trans. Image Process. 25, 3683–3697. https://doi.org/10.1109/TIP.2016.2567075 ï

[2] Sfeir, R., Michetti, J., Chebaro, B., Diemer, F., Basarab, A., Kouame, D., 2018. *Dental root canal segmentation from super-resolved 3D cone beam computed tomography data*, in: 2017 IEEE Nuclear Science Symposium and Medical Imaging Conference, NSS/MIC 2017 – Conference Proceedings. pp. 1–2. https://doi.org/10.1109/NSSMIC.2017.8533054

[3] Yang, J., Huang, T., 2010. *Image super-resolution: Historical overview and future challenges*.

[4] Tai, Y.W., Liu, S., Brown, M.S., Lin, S., 2010. *Super resolution using edge prior and single image detail synthesis*, in: Proceedings of the IEEE Computer Society Conference on Computer Vision and Pattern Recognition. https://doi.org/10.1109/CVPR.2010.5539933

[5] Blu, T., Blu, T., Unser, M., 2000. *Image Interpolation and Resampling*. Handb. Med. IMAGING, Process. Anal. 393–420.

[6]   Zhang, X., Wu, X., 2008. *Image interpolation by adaptive 2-D autoregressive modeling and soft-decision estimation*. IEEE Trans. Image Process. https://doi.org/10.1109/TIP.2008.924279

[7]   Mallat, S., Yu, G., 2010. *Super-resolution with sparse mixing estimators.* IEEE Trans. Image Process. https://doi.org/10.1109/TIP.2010.2049927

[8]   Freeman, W.T., Pasztor, E.C., Carmichael, O.T., 2000. *Learning low-level vision*. Int. J. Comput. Vis. https://doi.org/10.1023/A:1026501619075

[9]   Zeyde, R., Elad, M., Protter, M., 2012. *On single image scale-up using sparse-representations*, in: Lecture Notes in Computer Science (Including Subseries Lecture Notes in Artificial Intelligence and Lecture Notes in Bioinformatics).

[10] Dong, C., Loy, C.C., He, K., Tang, X., 2014. *Learning a deep convolutional network for image super-resolution*, in: Lecture Notes in Computer Science (Including Subseries Lecture Notes in Artificial Intelligence and Lecture Notes in Bioinformatics).

[11] Yang, C.-Y., Ma, C., Yang, M.-H., 2014. *Single-Image Super-Resolution: A Benchmark*. Lect. Notes Comput. Sci. (including Subser. Lect. Notes Artif. Intell. Lect. Notes Bioinformatics).

[12] Ng, M.K., Weiss, P., Yuan, X., 2010. *Solving Constrained Total-variation Image Restoration and Reconstruction Problems via Alternating Direction Methods.* SIAM J. Sci. Comput.

[13] Sun, J., Xu, Z., Shum, H.-Y., 2008. Image Super-Resolution using Gradient Profile Prior. 26th IEEE Conf. Comput. Vis. Pattern Recognition, CVPR.

[14] Sun, J., Xu, Z., Shum, H.Y., 2011. *Gradient profile prior and its applications in image super-resolution and enhancement.* IEEE Trans. Image Process.

[15] Beck, A., Teboulle, M., 2009. *A fast iterative shrinkage-thresholding algorithm for linear inverse problems*. SIAM J. Imaging Sci. 2, 183–202.

[16] Mart ń, G., On, J.B.-D., 2015. Hyperspectral compressive acquisition in the spatial domain via blind factorization. ieeexplore.ieee.org 7th Worksh.

[17] Morin, R., Basarab, A., Kouam é, D., 2012. Alternating Direction Method of Multipliers Framework for Super-Resolution in Ultrasound Imaging. Proc. - Int. Symp. Biomed. Imaging. https://doi.org/10.1109/ISBI.2012.6235880

[18] Marquina, A., Osher, S., Osher, S.J., 2008. *Image Super-Resolution by TV-Regularization and Bregman Iteration Signal and Image Processing : applications to Laser interferometry and Magnetic resonance spectroscopy View project Non-local Retinex* View project Image Super-Resolution by TV-Regularization. J. Sci. Comput. 37, 367–382. https://doi.org/10.1007/s10915-008-9214-8

[19] Shi, F., Cheng, J., Wang, L. P.Y.-I. transactions on, 2015, U., 2015. *LRTV: MR image super-resolution with low-rank and total variation regularizations*. ieeexplore.ieee.org.

[20] Elad, M., Processing, A.F.-I. transactions on image, 1997, U., 1997. *Restoration of a single superresolution image from several blurred, noisy, and undersampled measured images*. webee.technion.ac.il.

[21] Farsiu, S., Robinson, D., Elad, M., Milanfar, P., 2004. *Advances and Challenges in Super-Resolution*. Int J Imaging Syst Technol 14, 47–57. https://doi.org/10.1002/ima.20007

[22] Glazistov, I., Petrova, X., 2018. *Superfast joint demosaicing and super-resolution*. Electron. Imaging. https://doi.org/10.2352/issn.2470-1173.2018.15.coimg-272

[23] Wei, Q., Dobigeon, N., Tourneret, J.Y., 2015. *Fast Fusion of Multi-Band Images Based on Solving a Sylvester Equation*. IEEE Trans. Image Process. https://doi.org/10.1109/TIP.2015.2458572

[24] Eberhard, A., 2012. *Transform ée de Fourier Discr ète Course*, Vol. 87, 2004.

Authors' Profiles

Rose Sfeir, female. She received the B.Sc. degree in pure mathematics from Lebanese University, Lebanon, in 2009, and the M.Sc. degree in probability and statistics from The University of Provence, Aix-Marseille 1, France in 2011. She is currently pursuing the Ph.D. degree. Her research interests include medical imaging and inverse problems of image processing.

Bilal Chebaro, male, is a Professor at the Lebanese University. PhD, Applied Math,Lebanese University, Beirut, Faculty of Science I-Dept. of Computer Science and Statistics.

Charbel Julien, male. He received his Ph.D. degree in Computer Science in 2008 from Lumière Lyon 2's University, France. He is an associate professor, lecturer at the Lebanese University, Fanar, Computer Science and Statistics Department. His research interests are in machine learning and image processing.